

Available online at https://link.springer.com/journal/42241 http://www.jhydrodynamics.com

Journal of Hydrodynamics, 2024 https://doi.org/10.1007/s42241-024-0008-8



Numerical study of the near-wall vortical structures in particle-laden turbulent flow by a new vortex identification method-Liutex

Farid Rousta^{1*}, Goodarz Ahmadi¹, Bamdad Lessani², Chaoqun Liu³

- 1. Department of Mechanical and Aerospace Engineering, Clarkson University, Potsdam, NY, USA
- 2. Mechanical Engineering and Engineering Science, The University of North Carolina at Charlotte, NC, USA
- 3. Department of Mathematics, University of Texas at Arlington, Arlington, TX, USA

(Received January 31, 2024, Revised February 27, 2024, Accepted February 28, 2024, Published online April 2, 2024)

©China Ship Scientific Research Center 2024

Abstract: This study investigates turbulent particle-laden channel flows using direct numerical simulations employing the Eulerian-Lagrangian method. A two-way coupling approach is adopted to explore the mutual interaction between particles and fluid flow. The considered cases include flow with particle Stokes number varying from St = 2 up to St = 100 while maintaining a constant Reynolds number of Re_z = 180 across all cases. A novel vortex identification method, Liutex (Rortex), is employed to assess its efficacy in capturing near-wall turbulent coherent structures and their interactions with particles. The Liutex method provides valuable information on vortex strength and vectors at each location, enabling a detailed examination of the complex interaction between fluid and particulate phases. As widely acknowledged, the interplay between clockwise and counterclockwise vortices in the near-wall region gives rise to low-speed streaks along the wall. These low-speed streaks serve as preferential zones for particle concentration, depending upon the particle Stokes number. It is shown that the Liutex method can capture these vortices and identify the location of low-speed streaks. Additionally, it is observed that the particle Stokes number (size) significantly affects both the strength of these vortices and the streaky structure exhibited by particles. Furthermore, a quantitative analysis of particle behavior in the near-wall region and the formation of elongated particle lines was carried out. This involved examining the average fluid streamwise velocity fluctuations at particle locations, average particle concentration, and the normal velocity of particles for each set of particle Stokes numbers. The investigation reveals the intricate interplay between particles and near-wall structures and the significant influence of particles Stokes number. This study contributes to a deeper understanding of turbulent particle-laden channel flow dynamics.

Key words: Turbulent channel flow, particle-laden flow, direct numerical simulation (DNS), Eulerian-Lagrangian, vortex identification, turbulence coherent structures, Liutex

0. Introduction

In turbulent particle-laden flows, inertial particles tend to accumulate in the near-wall region. This phenomenon, known as the turbophoresis effect, results from the particles' inclination to migrate toward areas with lower fluctuation intensity. This tendency plays a key role in particle transport characteristics and particle deposition rates on the wall.

Numerical simulations offer an opportunity to investigate particle dispersion and deposition in wallbounded flows under various conditions. Among various numerical methods, the Eulerian-Lagrangian approach has been shown to provide accurate results

Biography: Farid Rousta, Male, Ph. D. Candidate **Corresponding author:** Farid Rousta,

E-mail: roustaf@clarkson.edu

for particle-laden turbulent flows^[1-3]. The method's accuracy is attributed to resolving the dispersed phase by tracking individual particles and its simplicity of modeling phase interaction. In this study, the direct numerical simulations (DNS) of particle-laden turbulent flow were performed using the Eulerian-Lagrangian model. The simulated flow and particle data were compiled and post-processed to provide a better understanding of flow and particle behaviors under various conditions. Particular attention was given to the near-wall vortical flow structures, particle concentrations, and their interactions. To fully understand the near-wall flow vortical structures, the first question that needs addressing is how to identify a vortex.

Various vortex identification methods have been introduced to study vortical structures in different fluid flow scenarios (e.g., Chakraborty et al. [4], Kolář^[5], Epps^[6]). Addressing the limitations of older-



generation vortex identification methods in distinguishing between vortex cores and shear motion, several new methods have been introduced in recent years. These include the Q- criterion^[7], Δ - criterion^[8], λ_{ci} - criterion^[9] and λ_2 - criterion^[9].

By modifying the Ω method and eliminating the dependency on a threshold, Liu et al. [10] introduced the Liutex (Rortex) method as a novel vortex identification technique. The core concept of the Liutex method involves defining a vortex core center or vortex rotation axis, where the change in vortex magnitude in directions other than the vortex rotation axis is zero.

In this study, the Liutex method was employed to examine the near-wall vortical structure of the fluid and its influence on near-wall particle dispersion. The primary objective was to assess the method's accuracy in identifying vortical structures, particularly the counter-rotating vortices that are responsible for the particle lineup in the near-wall region^[11]. The model's accuracy was examined, and the impact of particle Stokes number on their interactions with near-wall structures was studied. We provided insights into how particles with different Stokes numbers follow the flow in this region, how they disturb the flow, and how they deposit on the wall.

1. Governing equations and numerical methods

The continuity and momentum equations of the carrier fluid are written as:

$$\frac{\partial u_i}{\partial x_i} = 0 \tag{1}$$

$$\frac{\partial u_i}{\partial t} + u_j \frac{\partial u_i}{\partial x_i} = -\frac{1}{\rho} \frac{\partial p}{\partial x_i} + F \delta_{i1} + v \frac{\partial^2 u_i}{\partial x_i \partial x_i} - f_i$$
 (2)

where u_i is the fluid velocity, x_i is the ith spatial coordinate, ρ is fluid density and ν is fluid kinematic viscosity. The constant pressure gradient F drives the flow in the streamwise direction. The feedback terms, f_i account for the effect of particles on the carrier fluid in the momentum equation.

For the Lagrangian particle tracking, for simplicity, only the drag force is considered in the particle equation of motion, and the location and velocity of each particle as functions of time are evaluated. That is:

$$\frac{\mathrm{d}x_{ip}}{\mathrm{d}t} = v_i \tag{3}$$

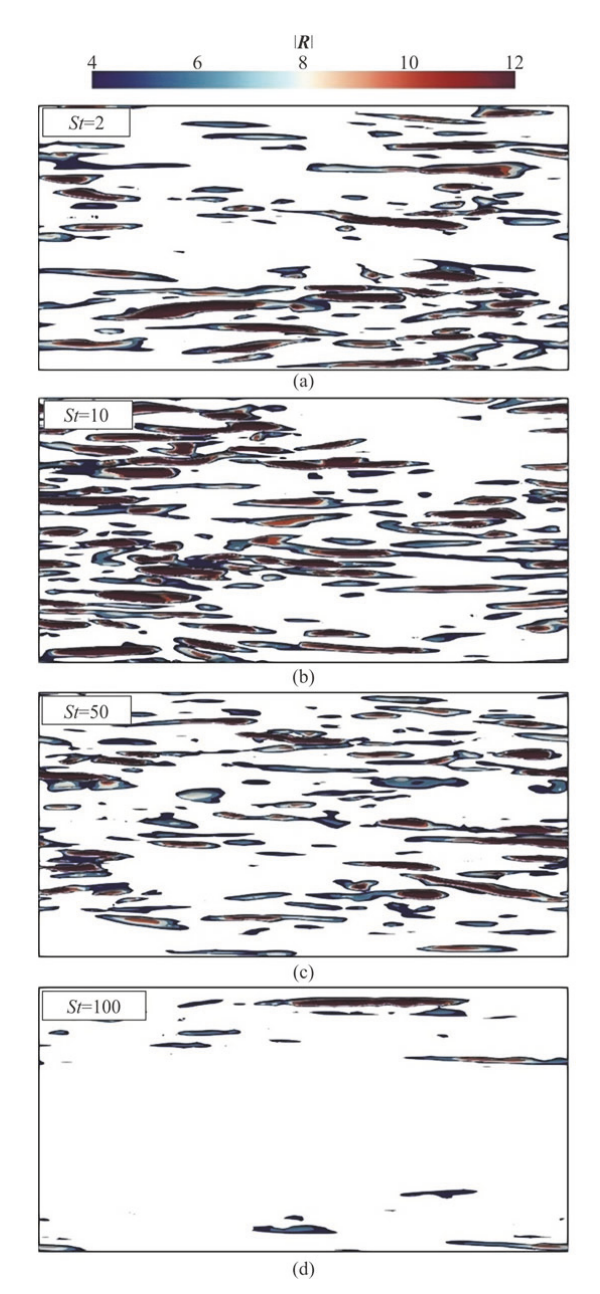


Fig. 1 Liutex strengths, |R|, for region of $(y^+<10)$. Liutex was calculated after averaging the velocity field for $tu_r/h=0.1$

$$\frac{\mathrm{d}v_i}{\mathrm{d}t} = \frac{u_i - v_i}{\tau_p} (1.0 + 0.15Re_p^{0.687}) \tag{4}$$

where x_{ip} is the particle position vector, v_i is particle velocity, $Re_p = |v_i - u_i| d_p / v$ is the particle Reynolds number and $|v_i - u_i|$ is the magnitude of particle velocity relative to the fluid velocity at the



particle position.

A second-order Adams-Bashforth method is used for the time integration of the particle equations, and a second-order Lagrange interpolation is used to calculate the fluid velocity at the particle location. For the flow equations, the convective terms of the momentum equation are discretized with a fourth-order central scheme in the periodic streamwise and spanwise directions and with a second-order central scheme in the wall-normal direction. A second-order central scheme is also used for viscous terms. An Adams-Bashforth method is used for the time integration of the momentum equation. A spectral method with a modified wave number is used for the pressure Poisson equation in the homogeneous direction combined with a tridiagonal solver for the normal direction. The solver can be run in parallel mode by dividing the computational domain into rectangular blocks in the normal direction^[12-14].

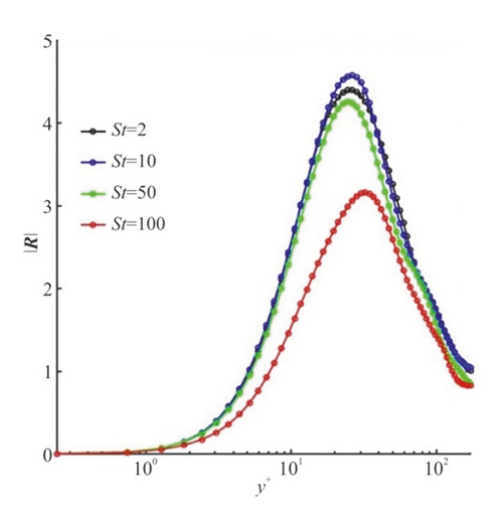


Fig. 2 (Color online) |R| averaged over time for $tu_r/h=10$ and the planes parallel to the wall

The dimensions of the computational domain in the streamwise x_1 , wall-normal x_2 and spanwise x_3 directions are $2\pi \times 2h \times \pi$, with h being the channel half-width. The adequacy of the size of the computational domain and grid element is verified by comparing the fluid statistics with previous DNS solutions in a larger domain of $4\pi h \times 2h \times 2\pi h$ (Kim et al. [15]) in Appendix A of Rousta and Lessani [14]. The fluid flow is simulated using a mesh of 128^3 grid points, uniformly distributed in the streamwise and spanwise directions and with a tangent hyperbolic distribution in the normal direction. The grid spacings in the streamwise and spanwise directions are $\Delta x_1^+ = 8.8$, $\Delta x_3^+ = 4.4$, and the first grid point away from the wall in the normal direction is located at

 $y^+ = x_{2\min}^+ = 0.2$, which is well below the thickness of the viscous sublayer for all cases.

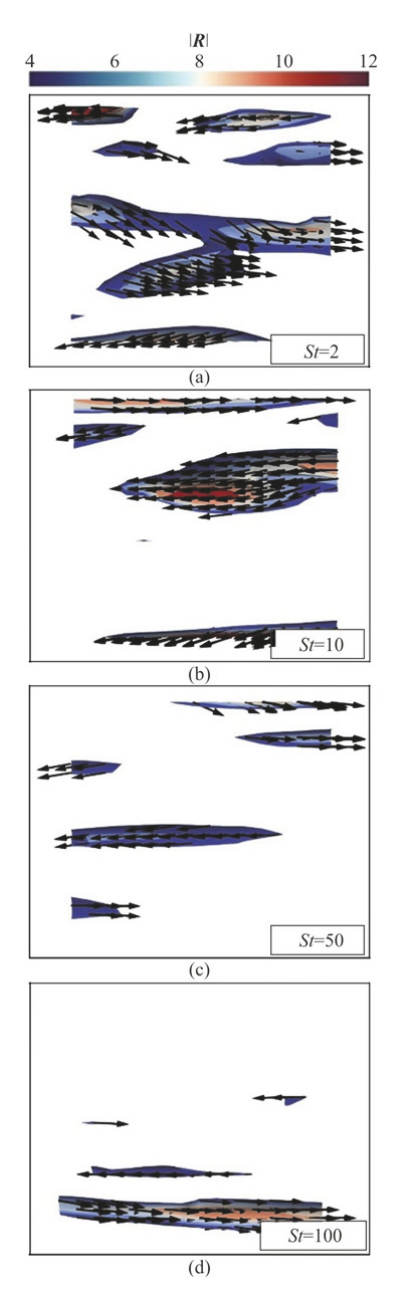


Fig. 3 Liutex vector, r, for the region of $(y^+ < 10)$ Liutex was calculated after averaging the velocity field for $tu_r/h = 0.1$

Table 1 presents the particle characteristics for all the cases under consideration. The *St* stands for the particle Stokes number, calculated as

$$St = \frac{\tau_p}{\tau_f} = \frac{\rho_p d_p^2 u_\tau^2}{18\mu\nu} \tag{5}$$



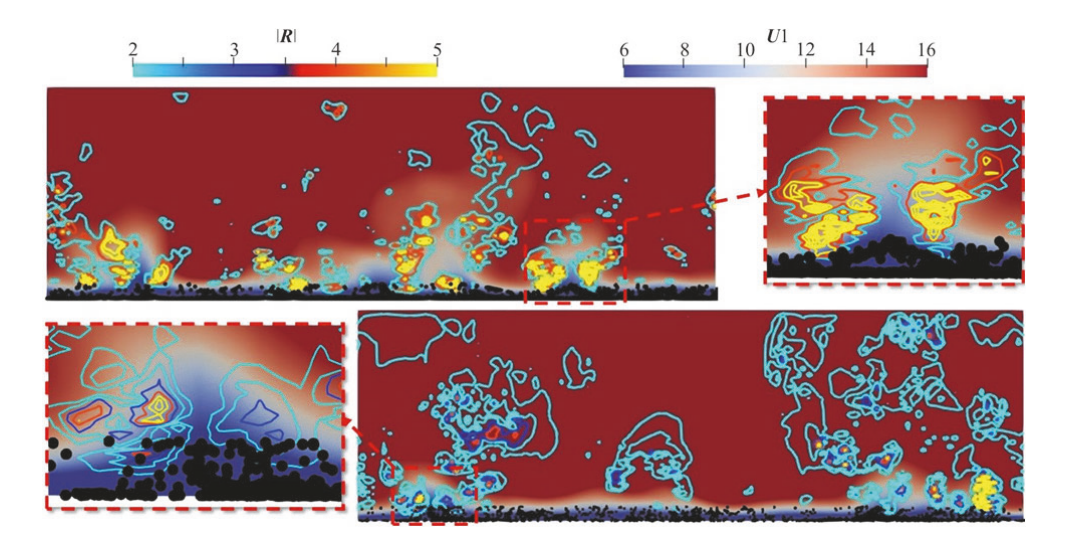


Fig. 4 (Color online) Streamwise velocity contour, U1, Liutex strength isolines, |R| from the wall to the center of the channel in the Y-Z plane, and particle dispersion for near-wall particles. The top contours depict the flow with St = 10 particles, while the bottom graphs illustrate the flow with St = 100 particles

where τ_f is the fluid time scale in wall units $(v/u_{\tau}^{2}), \ \tau_{p}$ is the relaxation time for particle velocity $(\rho_p d_p^2/18\mu)$, u_{τ} , ρ_p and d_p represent the friction velocity, particle density, and particle diameter. Also, the d_p^+ represents the diameter of particles in wall units, and φ_{v} denotes the particle volume fraction, which is the volume occupied by particles divided by the total volume of the domain. The total number of particles within the computational domain, denoted as $N_p = 2 \times 10^5$, remains constant across all cases. When a particle's distance from the wall is less than the particle radius, the particle is presumed to be adhered to the wall (trap-wall assumption). In such cases, the particle is substituted with a new particle randomly positioned within the domain^[3]

Table 1 Particle characteristics for all cases considered in this study

_	ti.	us study			
	St	d_p / h	d_p^+	$ ho_p$ / $ ho_f$	$\varphi_{_{_{\! \!$
	2	4×10 ⁻⁴	0.072	7 298	0.000017
	10	9×10^{-4}	0.162	7 298	0.000190
	50	20×10^{-4}	0.360	7 298	0.002100
	100	28×10^{-4}	0.504	7 298	0.005800

2. Vortex identification method

At each location, Liutex can be represented as $\mathbf{R} = R\mathbf{r}$, where R is the Liutex strength, the unit vector \mathbf{r} specifies its direction (Liutex vector).

2.1 Liutex vector

To determine the local rotational axis (direction

of Liutex or Liutex vector), the velocity gradient tensor, $\nabla \boldsymbol{u}$, needs to be transformed into a new coordinate system, ∇U , where the fluid rotational axis vector is parallel to the Z-axis (X_3 -axis)^[16].

It can be demonstrated $[^{[17-18]}$ that for any velocity gradient tensor, there exists a rotation matrix Q, where

$$\nabla U = Q \nabla u Q^{-1} \tag{6}$$

and

$$\frac{\partial U}{\partial Z} = 0, \quad \frac{\partial V}{\partial Z} = 0 \tag{7}$$

This implies that the only possible rotation vector in the new coordinate is in the X_3 -direction. Therefore, the Liutex vector would be aligned with the X_3 -axis of the new coordinate system.

2.2 *Liutex strength*

After computing the velocity gradient tensor in the new coordinate system, the Liutex strength (R) can be determined by [18-19]

$$R = 2(\beta - \alpha)$$
 if $\alpha^2 - \beta^2 < 0$, $\beta > 0$ (8a)

$$R = 2(\beta + \alpha)$$
 if $\alpha^2 - \beta^2 < 0$, $\beta < 0$ (8b)

$$R = 0 \quad \text{if} \quad \alpha^2 - \beta^2 \ge 0 \tag{8c}$$

where



$$\alpha = \frac{1}{2} \sqrt{\left(\frac{\partial V}{\partial Y} - \frac{\partial U}{\partial X}\right)^2 + \left(\frac{\partial V}{\partial X} + \frac{\partial U}{\partial Y}\right)^2} ,$$

$$\beta = \frac{1}{2} \left(\frac{\partial V}{\partial X} - \frac{\partial U}{\partial Y}\right)$$
(9)

3. Numerical results

In this section, the results of the Liutex method are presented for each case. The accuracy of the model in visualizing turbulent coherent structures in the near-wall region is also examined by comparing the results with particle dispersion and the fluid velocity field. As demonstrated earlier, the Liutex method provides a vortex as a vector $\mathbf{R} = R\mathbf{r}$, at each location with strength and direction.

Figure 1 illustrates the vortex strength |R| in the near-wall region $y^+ < 10$ for the four considered cases. From Fig. 1, it can be concluded that an increase in particle Stokes number initially amplifies the strength of vortices in the near-wall region, peaking at St = 10, and subsequently diminishes them with further increases in the Stokes number, reaching the lowest value at St = 100 for the range of Stokes number studied. It should be mentioned that the total number of particles and their density remains constant through all considered cases. Therefore, a higher particle Stokes number indicates a larger particle size and a higher mass loading of particles.

The results depicted in Fig. 1 were obtained through small-time averaging with $tu_{\tau}/h = 0.1$. To assess the accuracy of the conclusions drawn from this figure, Fig. 2 illustrates the time-averaged $(tu_{\tau}/h = 10)$ Liutex strength as a function of the distance from the wall.

Figure 2 shows that for the two-way coupled turbulent-laden flows, the Liutex strength is zero at the wall, increases in the near-wall region with distance from the wall, reaches its maximum at y^+ of about 25 to 40 depending on the Stokes number, and then decreases toward the center of the channel. It is seen that the Liutex strength is highest for the Stokes number of 2 to 10 and decreases as St further increases. In particular, the Liutex strength drops markedly for St = 100. This is because of the high mass fraction of these particles and their large size that damps the turbulence. Finally, near zero strength for Liutex in viscous sublayer points to the method's success in eliminating the contamination by shearing in the identification of the vortices.

Figure 2 also shows that the maximum Liutex

strength occurs for St = 10 particles (blue line), while the lowest is observed for St = 100 (red line), consistent with the observations in Fig. 1. In addition, the peak Liutex strength values occur at $y^+ \sim 25$, indicating the location of the core of vortex tubes in the near-wall region. This observation is consistent with prior research findings that indicate counterrotating vortices repeat every 100 wall units^[20-22], signifying that vortex tubes have a diameter of about 50 wall units^[23].

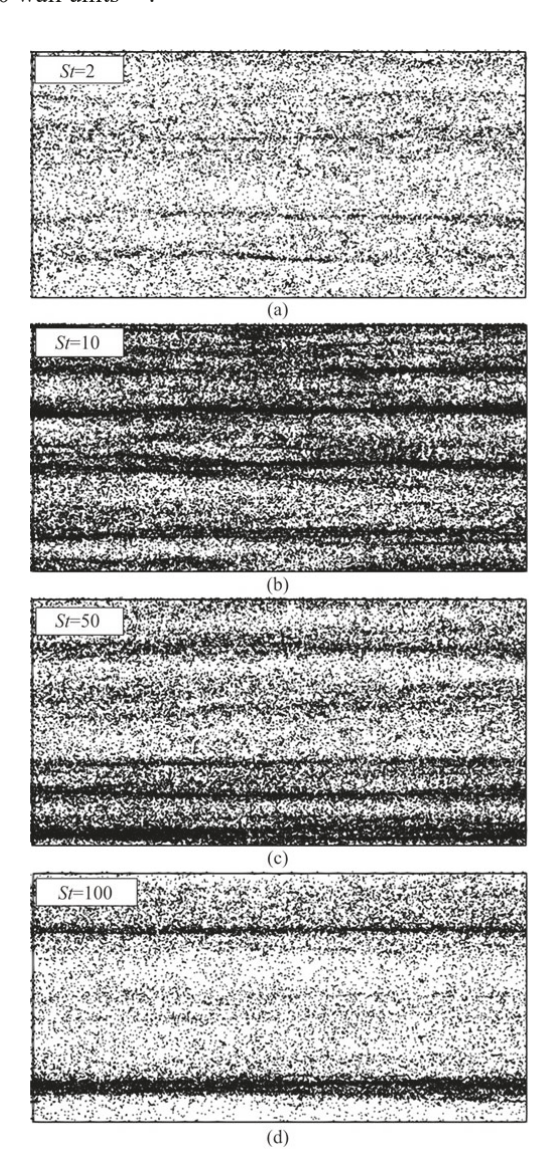


Fig. 5 Snapshot of particle dispersion in the near-wall region $(y^+ < 10)$ for all simulation cases. The percentage of particles in this region relative to the total number of particles in the channel is 17.6%, 64.7%, 46.7%, 26.6% for St = 2, 10, 50, 100

Figure 3 shows the Liutex vector alongside the



Liutex strength isosurfaces in a channel section in the wall region $(y^+ < 10)$. This figure indicates that the majority of vectors are aligned in the streamwise direction but with opposite orientations, which is attributed to the presence of counter-rotating vortices.

To examine particle interaction with near-wall vortices, Fig. 4 depicts the flow in a spanwise-normal plane from the wall up to the channel center. In this figure, the background contour represents the streamwise velocity, the isolines depict the Liutex strength, and black dots indicate particles in the region $(v^+ < 10)$.

The zoomed-in sections of each graph highlight the precision of the vortex identification method in capturing the near-wall structure. Two interacting vortices are observed, resulting in ejection motions that uplift the low-speed flow from the wall, consequently generating low-speed streaks. Notably, a similar phenomenon occurs with particles, where these counter-rotating vortices uplift the particles from the near-wall region, creating the elongated particle lines illustrated in Fig. 5.

Figure 5 displays a snapshot of particle dispersion in the near-wall region of the channel. Particles with St = 2 loosely follow the near-wall structure and do not exhibit clear particles streaky structure. St = 10 particles, which have the highest Liutex strength (see Fig. 2), show the greatest concentration in the near-wall region. Given that the total spanwise length of the channel is $z^+ = 565$, it is observed that elongated particle lines occur at distances of approximately 100 wall units from each other for St = 10, which is the known spacing on the near-wall coherent structures.

St=100, which appears to have the lowest concentration in the near-wall region, surprisingly has the highest concentration of particles in low-speed streaks. As shown in Fig. 4, these elongated particle lineups occur in low-speed streaks uplifted by the ejection mechanism resulting from the interaction of counterrotating vortices. Therefore, the proportion of particles in elongated lines can be quantified by examining the fluid streamwise velocity at their locations. The streamwise velocity fluctuations at particle locations can be calculated as $u'|_{@p} = u_1|_{@p} - \langle u_1 \rangle$ representing the fluid velocity at the particle location minus the average fluid velocity at that X - Z (streamwise-spanwise) plane.

Figure 6 presents the $u'|_{@p}$ averaged over time and the total number of particles at the X-Z plane (conditional mean). Except for the channel core region, the conditional mean, $\langle u'|_{@p} \rangle$, is negative along the channel width, confirming the accumulation of

particles in low-speed streaks. In all cases, the minimum value of $\langle u'|_{@_p} \rangle$ occurs above the viscous

sub-layer and around $y^+ \approx 10$, which is 10 to 20 wall units below the core of vortex tubes, as expected from Fig. 4. Figure 6 also shows that the accumulation of particles in low-speed streaks first increases with the particle Stokes number from St = 2 to St = 10. Furthermore, increasing the Stokes number from St = 10 to St = 50 decreases the number of particles in the elongated structures. Further increase of St = 50 to St = 100 again decreases the number of accumulation of particles in low-speed streaks.

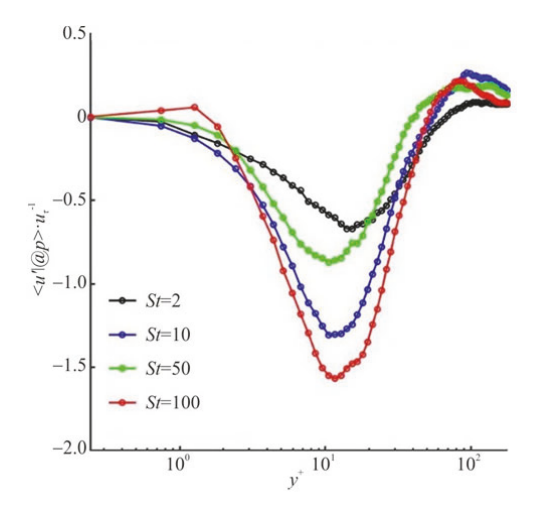


Fig. 6 (Color online) Variations of the conditional mean of fluid streamwise fluctuations at particle locations, $\left\langle u_1'\right|_{@p}\right\rangle$

This can be clarified by considering particle concentration, particle deposition velocity, and particle average normal velocity. Figure 7 illustrates that the particle's normal velocity near the wall is significantly low for low-inertia particles. Consequently, it can be inferred that the particles deposited on the wall originate from those trapped in the near-wall region. A comparison between St = 2 and St = 10 particles reveals that the turbophoresis effects, which bring particles toward the walls, are more pronounced for St = 10, as indicated by its higher normal velocity, resulting in a higher particle concentration and deposition velocity for St = 10. For higher inertia particles (St = 50, St = 100), the normal velocity of particles near the wall is orders of magnitude larger compared to low inertia particles. Therefore, the deposited particles come from the outer region. Larger particles originating from the outer region lead to more damping of near-wall low-strength vortices, as observed in Fig. 1 for St = 100. Comparing the St = 50,



St = 100 particles, St = 50 lacks the momentum of St = 100 to escape the viscous sublayer, trapping a significant portion of them in the near-wall region, resulting in higher near-wall concentration and lower deposition velocity for St = 50 compared to St = 100.

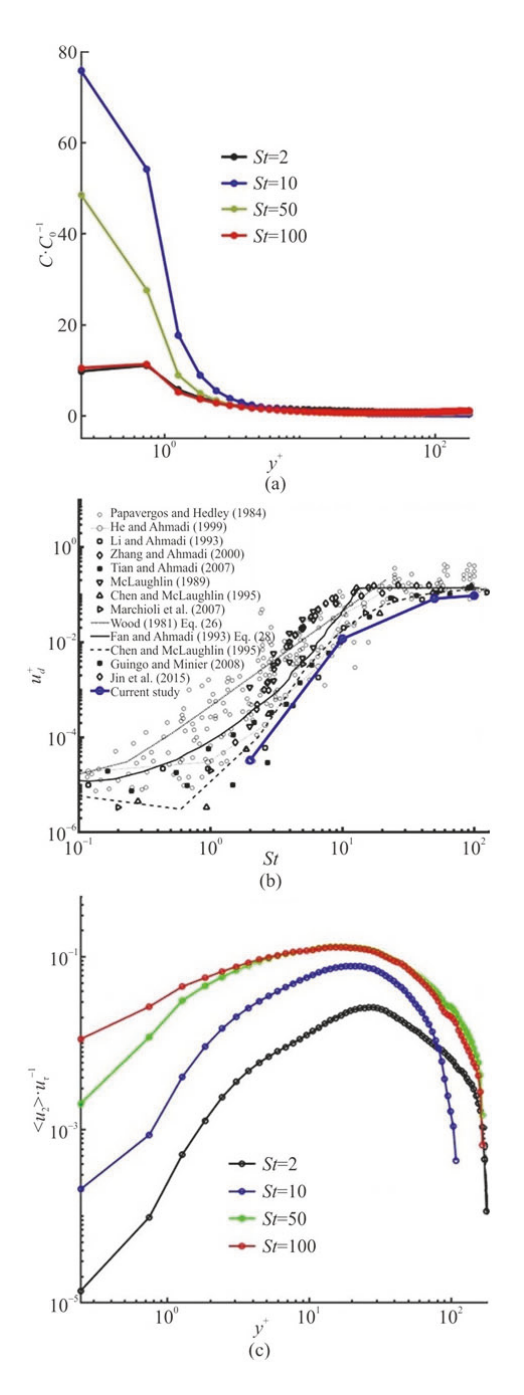


Fig. 7 (Color online) (a) Time and local average particle concentration, (b) Particle deposition velocity, (c) Average particle normal velocity for all considered cases

4. Conclusions

In this investigation, a numerical simulation of particle-laden turbulent channel flow was conducted using the DNS approach. The Eulerian equations governing fluid flow were solved, and Lagrangian particle tracking, with drag force as the primary acting force on particles, was employed to simulate the particulate phase. The two-way coupling between particles and fluid flow was considered, and particles' interaction with the wall was modeled as fully absorbing (trap-wall) to achieve statically steady-state conditions. Simulations were conducted for particles with Stokes numbers (St) of 2, 10, 50 and 100 while maintaining a constant friction Reynolds number of $Re_r = 180$.

The Liutex (Rortex) vortex identification method was employed to analyze near-wall turbulent coherent structures and their interaction with particles. It was shown that the Liutex method effectively captured counter-rotating vortices responsible for low-speed streaks in the near-wall region, where particles exhibited a tendency to concentrate in elongated lines.

It was shown that the Liutex strength in the nearwall region is maximum for particles with St = 10, while particles with St = 100 exhibit the minimum Liutex strength in the near-wall region. This difference is attributed to the damping effect caused by higher inertia and high mass fraction of particles with St = 100, reducing the strength of the near-wall vortices. The Liutex vectors in locations with high Liutex strengths align in the streamwise direction, indicating elongated vortex tubes in the streamwise direction. The tendency of particles to accumulate in low-speed streaks was also examined through snapshots of particle dispersion in the near-wall region and using the conditional mean of fluid streamwise fluctuations at particle locations for each set of particles. It was observed that, although St = 10particles exhibit the highest concentration in the nearwall region and a more defined particle accumulation lines in low-speed streaks, a higher percentage of particles with St = 100 accumulate into the lowspeed streaks compared with the total number of particles in that region. From this observation, it is concluded that despite the marked damping effect for St = 100 particles, the counter-rotating vortices retained sufficient strength to trap a majority of particles in low-speed streaks.

An analysis of particle deposition velocity and particles' normal velocity showed that low inertia particles primarily deposit on the wall after getting trapped in streaky structures, given their very low normal velocity. Conversely, for higher inertia particles, the normal velocity in the near-wall region is several orders of magnitude higher than that of low



inertia particles, indicating their origin from the outer region and justifying the low Liutex strength for St = 100 particles. The results provided in this study enhanced our understanding of particle dispersion in the channel and their interaction with near-wall coherent structures.

Acknowledgments

Some of the computing for this project was performed on the ACRES cluster. We would like to thank Clarkson University and the Office of Information Technology for providing computational resources and support that contributed to these research results.

Compliance with ethical standards

Conflict of interest: The authors declare that they have no conflict of interest. Chaoqun Liu is editorial board member for the Journal of Hydrodynamics and was not involved in the editorial review, or the decision to publish this article. All authors declare that there are no other competing interests.

Ethical approval: This article does not contain any studies with human participants or animals performed by any of the authors.

Informed consent: Not applicable.

References

- Fan F. G., Ahmadi G. A sublayer model for turbulent deposition of particles in vertical ducts with smooth and rough surfaces [J]. *Journal of Aerosol Science*, 1993, 24: 45-64.
- [2] Soltani M., Ahmadi G., Ounis H. et al. Direct simulation of charged particle deposition in a turbulent flow [J]. International journal of multiphase flow, 1998, 24: 77-92.
- [3] Rousta F., Lessani B., Ahmadi G. Particle dispersion and deposition in wall-bounded turbulent flow [J]. *Interna*tional Journal of Multiphase Flow, 2023, 158: 104307.
- [4] Chakraborty P., Balachandar S., Adrian R. J. On the relationships between local vortex identification schemes [J]. *Journal of Fluid Mechanics*, 2005, 535: 189-214.
- [5] Kolář V. Vortex identification: New requirements and limitations [J]. *International Journal of Heat and Fluid Flow*, 2007, 28(4): 638-652.
- [6] Epps B. Review of vortex identification methods [C]. 55th AIAA Aerospace Sciences Meeting, Dallas, USA, 2017.
- [7] Hunt J., Wray A., Moin P. Eddies, streams, and convergence zones in turbulent flows [R]. Proceedings of the Summer Program. Center for Turbulence Research Report CTR-S88, 1988, 193-208.

- [8] Chong M. S., Perry A. E., Cantwell B. J. A general classification of three-dimensional flow fields [J]. *Physics* of Fluids A: Fluid Dynamics, 1990, 2: 765-777.
- [9] Zhou J., Adrian R. J., Balachandar S. et al. Mechanisms for generating coherent packets of hairpin vortices in channel flow [J]. *Journal of Fluid Mechanics*, 1999, 387: 353-396.
- [10] Liu C., Wang Y., Yang Y. et al. New omega vortex identification method [J]. Science China Physics, Mechanics and Astronomy, 2016, 59(8): 684711.
- [11] Soldati A., Marchioli C. Physics and modelling of turbulent particle deposition and entrainment: Review of a systematic study [J]. *International Journal of Multiphase* Flow, 2009, 35: 827-839.
- [12] Rousta F., Lessani B. Near-wall heat transfer of solid particles in particle-laden turbulent flows [J]. *International Communications in Heat and Mass Transfer*, 2020, 112: 104475.
- [13] Rousta F., Lessani B. Direct numerical simulation of turbulent particle-laden flows: Effects of Prandtl and Stokes numbers [J]. *International Journal of Heat and Mass Transfer*, 2021, 166: 120724.
- [14] Rousta F., Lessani B. Numerical study of thermally developing turbulent internal flows [J]. *International Journal of Heat and Mass Transfer*, 2022, 188: 122623.
- [15] Kim J., Moin P., Moser R. Turbulence statistics in fully developed channel flow at low Reynolds number [J]. *Journal of Fluid Mechanics*, 1987, 177: 133-166.
- [16] Tian L., Ahmadi G. Particle deposition in turbulent duct flows-comparisons of different model predictions [J]. *Journal of Aerosol Science*, 2007, 38(4): 377-397.
- [17] Liu C., Yu Y. Mathematical foundation of liutex theory [J]. *Journal of Hydrodynamics*, 2022, 34(6): 981-993.
- [18] Liu C., Gao Y., Tian S. et al. Rortex-A new vortex vector definition and vorticity tensor and vector decompositions [J]. *Physics of Fluids*, 2018, 30(3): 035103.
- [19] Wang Y. Q., Gao Y. S., Liu J. M. et al. Explicit formula for the liutex vector and physical meaning of vorticity based on the liutex-shear decomposition [J]. *Journal of Hydrodynamics*, 2019, 31(3): 464-474.
- [20] Kim J., Moin P., Moser R. Turbulence statistics in fully developed channel flow at low Reynolds number [J]. *Journal of Fluid Mechanics*, 1987, 177: 133-166.
- [21] Ounis H., Ahmadi G., McLaughlin J. B. Brownian particle deposition in a directly simu- lated turbulent channel flow [J]. *Physics of Fluids A: Fluid Dynamics*, 1993, 5: 1427-1432.
- [22] Zhang H., Ahmadi G. Aerosol particle transport and deposition in vertical and horizontal turbulent duct flows [J]. *Journal of Fluid Mechanics*, 2000, 406: 55-80.
- [23] Nasr H., Ahmadi G., McLaughlin J. B. A DNS study of effects of particle–particle collisions and two-way coupling on particle deposition and phasic fluctuations [J]. *Journal of Fluid Mechanics*, 2009, 640: 507-536.

